

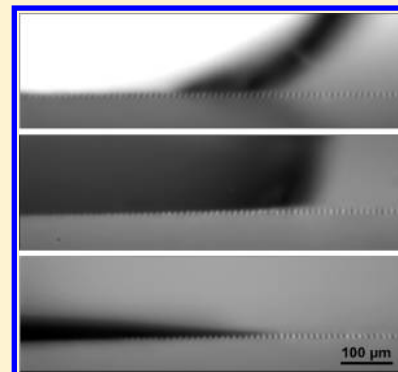
# Wetting and Dewetting Transitions on Hierarchical Superhydrophobic Surfaces

Jonathan B. Boreyko, Christopher H. Baker, Celeste R. Poley, and Chuan-Hua Chen\*

Department of Mechanical Engineering and Materials Science, Duke University, Durham, North Carolina 27708, United States

**S** Supporting Information

**ABSTRACT:** Many natural superhydrophobic structures have hierarchical two-tier roughness which is empirically known to promote robust superhydrophobicity. We report the wetting and dewetting properties of two-tier roughness as a function of the wettability of the working fluid, where the surface tension of water/ethanol drops is tuned by the mixing ratio, and compare the results to one-tier roughness. When the ethanol concentration of deposited drops is gradually increased on one-tier control samples, the impalement of the microtier-only surface occurs at a lower ethanol concentration compared to the nanotier-only surface. The corresponding two-tier surface exhibits a two-stage wetting transition, first for the impalement of the microscale texture and then for the nanoscale one. The impaled drops are subsequently subjected to vibration-induced dewetting. Drops impaling one-tier surfaces could not be dewetted; neither could drops impaling both tiers of the two-tier roughness. However, on the two-tier surface, drops impaling only the microscale roughness exhibited a full dewetting transition upon vibration. Our work suggests that two-tier roughness is essential for preventing catastrophic, irreversible wetting of superhydrophobic surfaces.



## 1. INTRODUCTION

Natural superhydrophobic surfaces, such as lotus leaves<sup>1</sup> and water strider legs,<sup>2</sup> are known for their ability to completely repel water. These superhydrophobic surfaces are characterized by low-energy surface roughness, such that water drops rest on top of the texture and trap air underneath, resulting in drops exhibiting large apparent contact angles ( $\geq 150^\circ$ ) and small contact angle hysteresis ( $\leq 10^\circ$ ).<sup>3</sup> Such highly mobile drops are in the Cassie–Baxter state,<sup>4</sup> which is opposite to the Wenzel state, where drops penetrate into the surface cavities, resulting in lower apparent contact angles and larger hysteresis.<sup>5</sup> Interestingly, while Cassie drops have been successfully obtained on engineered substrates composed of only micropillars<sup>6,7</sup> or only nanopillars,<sup>8,9</sup> most known examples of natural superhydrophobic surfaces exhibit a hierarchical roughness comprised of both microscale and nanoscale features.<sup>1,10</sup>

To better understand the importance of hierarchical roughness, it is useful to consider the fragility of the superhydrophobic Cassie state. For example, it was observed that Cassie drops can permanently collapse into impaled Wenzel drops when experiencing external pressure,<sup>6,11</sup> evaporation to a higher Laplace pressure,<sup>12,13</sup> impact against the surface,<sup>14</sup> or mechanical vibration.<sup>15</sup> Furthermore, dew drops condensing within a superhydrophobic surface were found to naturally form in a Wenzel or mixed Wenzel–Cassie state.<sup>11,16–18</sup> It has been shown that hierarchical surfaces, when compared to corresponding surfaces with only microscale or only nanoscale roughness, exhibit superior superhydrophobicity for deposited drops,<sup>19,20</sup> evaporating drops,<sup>20,21</sup> and condensed drops.<sup>22</sup> Although the mechanism is

not entirely clear, the Cassie state is known to become more robust (i.e., energetically stable) with two-tier roughness, therefore increasing resistance against impalement to the undesirable Wenzel state.<sup>23–26</sup>

Resisting wetting transitions is certainly a key feature of robust superhydrophobicity, but an equally important yet often ignored criterion is the ability to enable dewetting transitions. Removal of sticky Wenzel drops, such as condensing dew, from a surface is highly desired but hard to achieve.<sup>27</sup> Antidew superhydrophobicity is challenging because condensing dew drops tend to impale the (microscale) surface texture, resulting in the sticky Wenzel state, even on two-tier superhydrophobic surfaces where the Cassie state is the energetically stable configuration.<sup>28</sup> It was reported that the Wenzel to Cassie dewetting transition for sticky dew drops can be successfully achieved on such surfaces by employing mechanical vibration for millimetric drops<sup>29</sup> and even via naturally occurring droplet coalescence for micrometric drops (at this length scale the surface energy released upon coalescence is enough to launch merging drops off the surface).<sup>30,31</sup>

In this work, we investigate the wetting and dewetting transitions of drops on synthetic one-tier and two-tier superhydrophobic surfaces with controlled surface roughness. We report the presence of two-stage wetting transitions on the two-tier surface, and show the intermediate case of wetting only one level of roughness. Compared to other wetting studies of hierarchical structures, our approach is unique in the use of a liquid mixture

Received: October 26, 2010

Published: May 23, 2011

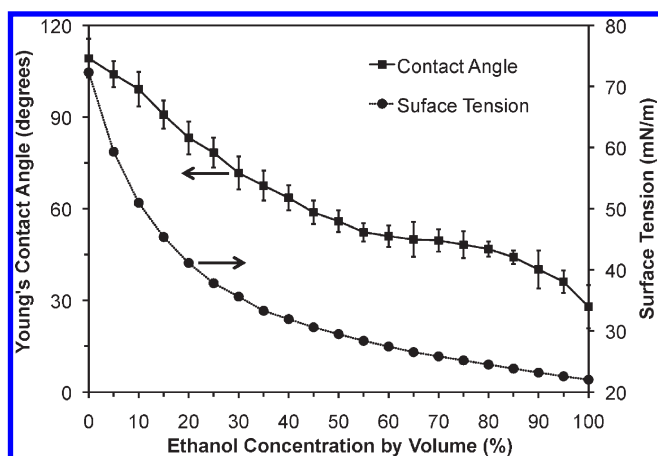


**Figure 1.** The Young's contact angle ( $\theta_Y$ ) on a smooth surface as a function of the ethanol concentration by volume. The corresponding surface tension is plotted from ref 32.

with wetting properties that are continuously tunable by its composition, which clearly reveals the two distinct wetting stages associated with each tier of surface roughness. Our work is also unique in linking the wetting states to dewetting transitions. We show that the dewetting transition from the Wenzel to Cassie state is possible when only the microtier is wetted on the two-tier surface, but not possible when both tiers are impaled or when a one-tier surface is impaled.

## 2. MATERIALS AND METHODS

Wetting and dewetting transitions of aqueous drops on a surface with two-tier roughness were studied with one-tier surfaces as control cases. The wettability of the working fluid was tuned by the mixing ratio of water and ethanol.

**2.1. Superhydrophobic Surfaces.** A two-tier surface composed of dry-etched silicon micropillars and vertically deposited carbon nanotubes was prepared in the same manner as structure  $B_{mn}$  from ref 22 (see the inset in Figure 5a). To serve as control cases, one-tier surfaces composed of only micropillars (Figure 2a, inset) or only nanotubes (Figure 3a, inset) were also fabricated and were geometrically equivalent to their two-tier counterparts to within 10%. Note that the carbon nanotubes capped with catalyst were effectively nanofibers.

All surfaces reported here were coated with a 10 nm layer of gold and then a monolayer of 1-hexadecanethiol (Fluka 52270). On a smooth silicon wafer treated with the same process, the Young's contact angle of the alkylthiol coating was measured as a function of ethanol concentration (Figure 1). Drops were  $2.5 \mu\text{L}$  in volume and deposited with successive increments of 2.5% ethanol concentration. The corresponding decrease in the liquid–vapor surface tension was taken from the literature.<sup>32</sup>

**2.2. Wetting Methods.** To study the wetting states of the one- and two-tier surfaces, the apparent contact angle of deposited drops was measured as a function of ethanol concentration. Rather than continuously raising the ethanol concentration of a single drop, which is difficult to accomplish, a series of drops were separately deposited with successive increments of 2.5% ethanol concentration by volume, until the surface was completely wetted. The droplet volume was typically  $2.5 \mu\text{L}$  to minimize gravitational effects, and each drop was photographed within the first 10 s of deposition to minimize the effects of solvent evaporation. For very small contact angles, the volume of the drop was reduced down to  $1 \mu\text{L}$  to ensure imaging of the entire drop. Between 1 and  $2.5 \mu\text{L}$ , the drop volume had negligible effect on the contact angle

measurement. Imaging was performed with a Cooke Pixelfly QE camera attached to an Infinity K2/S long-distance microscope.

For the two-tier surface, contact angle hysteresis was additionally measured with successive increments of 5.0% ethanol. To measure the contact angle hysteresis, a drop deposited on a smooth hydrophilic glass substrate was inverted and brought into contact with the rough substrate. While the two substrates were held parallel, the glass substrate was laterally displaced until the drop started to slide on the rough surface, at which point the advancing and receding contact angles were recorded.<sup>11</sup>

Because of the uncertainties associated with the preferential ethanol evaporation, 2.5% increments in ethanol concentration was about the minimum interval that was still meaningful given the experimental uncertainties. For measurements of contact angle hysteresis, longer evaporation time (up to 30 s) was needed before accurate measurements could be taken; therefore, a 5% increment was chosen. Five independent measurements were performed for each contact angle and three for each contact angle hysteresis. All uncertainties were reported at the 95% confidence interval.

**2.3. Dewetting Methods.** The dewetting transitions were studied with mechanical vibration.<sup>29</sup> The superhydrophobic substrates were fixed to a horizontal flat plate attached to a vertically vibrating speaker cone (KLH Audio B-Pro6). Drops impaled into the rough substrates were allowed to evaporate for a predetermined time and then subjected to mechanical vibration. For the drop volumes used in the dewetting experiments, a frequency of 100 Hz was used because of its proximity to the second resonance mode.<sup>29,33</sup> The laboratory was at 51% relative humidity and 21 °C. High-speed imaging was performed with a Phantom v7.1 camera to visualize the dewetting process, if any.

Before mechanical vibration was initiated for the two-tier surface, the impaled drops were allowed to evaporate until they followed the  $d^2$ -law;<sup>34</sup> i.e., the diameter squared decreased linearly with time. The observance of the  $d^2$ -law indicated that the evaporated drop was dominated by a single component, in this case water, which evaporates about 5 times slower than ethanol. See the Supporting Information of ref 29 for more details. Using this approach, a water–ethanol drop can (partially) impale the two-tier surface when initially deposited; upon preferential evaporation of the ethanol, the predominantly water drop can undergo vibration-induced dewetting to the Cassie state, which is energetically favorable for pure water.

## 3. WETTING TRANSITIONS

The wetting states on rough surfaces were studied as a function of the wettability of the aqueous working fluid, which was tuned by ethanol with different mixing ratios. To facilitate interpretation of the two-stage wetting process on the two-tier surface, one-tier surfaces corresponding to either the microtier or the nanotier were studied first.

**3.1. One-Tier Surfaces.** On simple one-tier surfaces, aqueous drops with increasing ethanol concentration were deposited and their contact angles were measured immediately upon deposition. As the ethanol concentration increased, the apparent contact angle on the micropillared surface exhibited a sudden decrease at  $11.25 \pm 1.25\%$  ethanol (Figure 2a), whereas the sudden change on the nanopillared surface occurred later at  $17.5 \pm 2.5\%$  (Figure 3a). To better show different wetting states, Figures 2a and 3a were transformed into cosine–cosine plots in Figures 2b and 3b, where the  $x$ -axis represents the cosine of the Young's contact angle on the smooth surface (see Figure 1) and the  $y$ -axis represents the cosine of the apparent contact angle on the roughened surface.

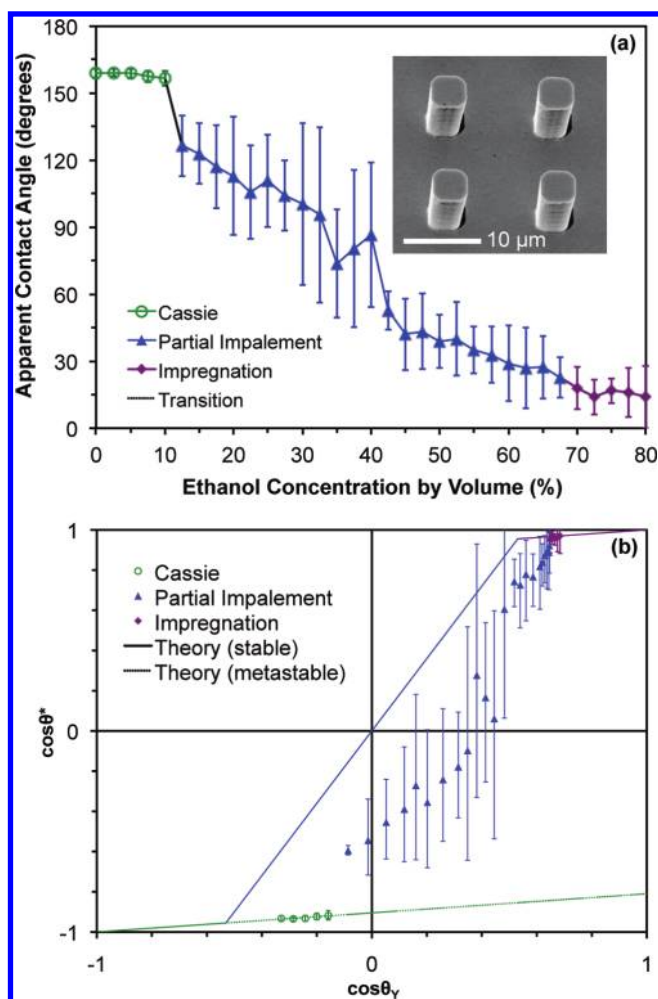


**Figure 2.** (a) Apparent contact angles of drops deposited on the micropillared surface, as a function of the ethanol concentration. A sharp wetting transition from the Cassie to Wenzel state occurred at  $11.25 \pm 1.25\%$  ethanol. (b) The same data replotted on a cosine–cosine map. Theoretical lines of the three wetting regimes (eqs 1–3) are solid when energetically stable and are dotted when metastable.

In the *Cassie state*, the apparent contact angle ( $\theta^*$ ) of drops completely suspended on one-tier surfaces is given by the Cassie–Baxter equation<sup>4</sup>

$$\cos \theta^* = \phi (\cos \theta_Y + 1) - 1 \quad (1)$$

where  $\theta_Y$  is the Young's contact angle on a corresponding smooth surface and  $\phi$  represents the solid fraction.<sup>3</sup> In the *Wenzel state*, the apparent contact angle of drops fully penetrated into one-tier surfaces is given by the Wenzel equation<sup>5</sup>

$$\cos \theta^* = r \cos \theta_Y \quad (2)$$

where  $r$  represents the surface roughness parameter.<sup>3</sup> For liquids with extremely high wettability, the *impregnation state* is possible and the superhydrophilic state follows:<sup>35</sup>

$$\cos \theta^* = \phi (\cos \theta_Y - 1) + 1 \quad (3)$$

In this superhydrophilic state, the cavities beneath and surrounding the drop are both fully wetted.<sup>3</sup>

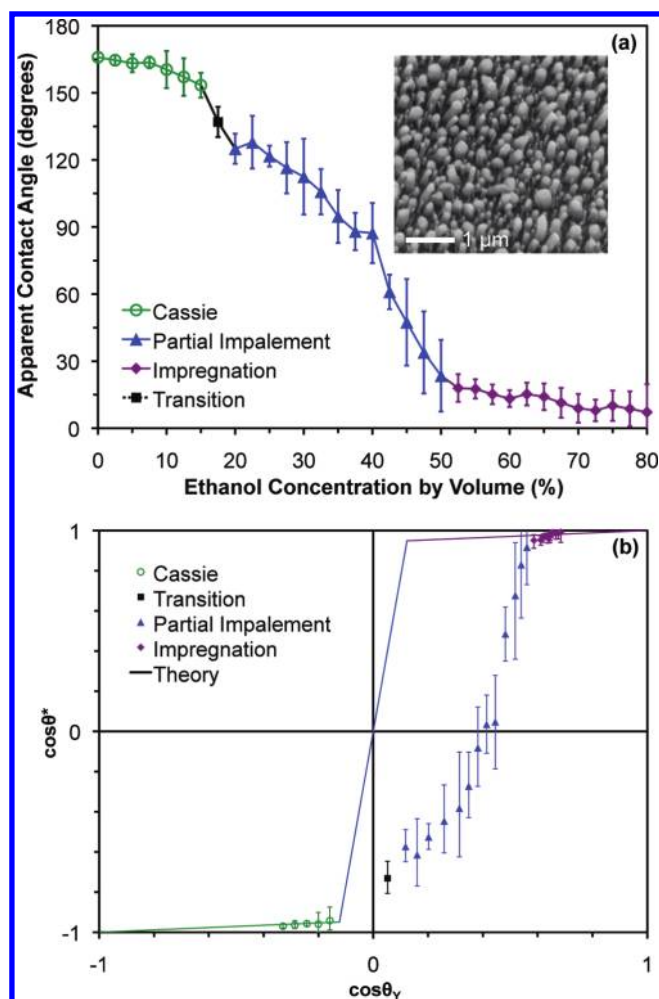


**Figure 3.** Apparent contact angles of drops deposited on the nanopillared surface, as a function of the ethanol concentration. The Cassie and Wenzel states are separated by a brief wetting transition around  $17.5 \pm 2.5\%$  ethanol. (b) The same data replotted on a cosine–cosine map, overlaid with theoretical lines of the three wetting regimes (eqs 1–3). Due to the ambiguity in measuring the solid fraction ( $\phi_n$ ) for nanotubes of nonuniform height, the effective solid fraction was extrapolated from a linear fit to the data in the Cassie regime.

In Figures 2b and 3b, the experimental data were compared with eqs 1–3. The geometrical parameters were calculated from geometrical measurements reported in ref 22, except for the nanoscale solid fraction ( $\phi_n$ ). For the nanotier-only surface, the height variation of the nanotubes was significant (up to one-fourth of the average height); in addition, the caps of the nanotubes were not exactly flat. Therefore, the nominal solid fraction of 25% based on the projected surface area<sup>22</sup> was an overestimate of the actual fraction of solid in contact with the suspended drop. With the lack of an accurate experimental measurement, we chose to fit the experimental data that apparently fell onto the Cassie regime, i.e., the contact angles in the third-quadrant that followed eq 1 (Figure 3b). This fitting procedure yielded an effective solid fraction of  $\phi_n = 0.058$ , which was used for all subsequent calculations involving the nanoscale solid fraction, including the two-tier surface.

Note that the nanotier solid fraction ( $\phi_n$ ) was the only geometrical parameter not directly measured. For the microtier-only

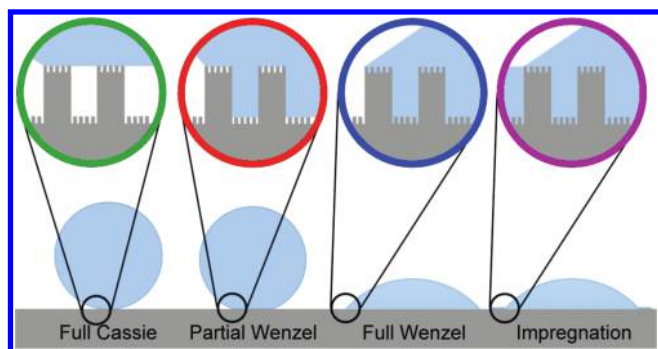


**Figure 4.** Wetting states (nonexhaustive) on a two-tier surface. In the full Cassie state, there is no liquid impalement into any cavity. In the partial impalement state, liquid impalement takes place, but not all cavities are completely filled; a special case of the partial impalement regime, the partial Wenzel state, exclusively refers to the “microtier Wenzel, nanotier Cassie” state in this paper. In the full impalement state, all the cavities are completely filled with liquid; both the full Wenzel and impregnation states belong to the full impalement regime, the latter signified by an impregnated liquid film surrounding the drop. Schematics are not to scale.

surface, no fitting parameter was used, but the experimental data perfectly fell onto the (metastable) Cassie state using the experimentally measured solid fraction ( $\phi_m$ ). The surface roughnesses ( $r_m$  and  $r_n$ ) were less susceptible to inhomogeneity of the micropillars or nanopillars and were taken from previous measurements.<sup>22</sup>

On one-tier surfaces, the experiments agreed well with the models for the superhydrophobic Cassie and superhydrophilic impregnation states. The stable Cassie state in Figure 3b and metastable Cassie state in Figure 2b both agreed with eq 1. The impregnation regime was well-predicted by eq 3 and was corroborated by an optically visible impregnation film surrounding the deposited drop, particularly apparent for the microtier surface. For both the microtier and nanotier surfaces, drops in between the Cassie state and the impregnation state exhibited an apparent angle bound by predictions from the metastable Cassie state (eq 1) and the Wenzel state (eq 2). This intermediate regime was fundamentally different from the Cassie state, because of a dramatically larger contact angle hysteresis, and from the impregnation state, because of the lack of visible prewetted cavities surrounding the drop.

We shall call the intermediate regime a *partial impalement state*, regardless of the microscopic configuration leading to the intermediate state. At least two configurations are plausible for the intermediate regime: (i) the drop wets the roughened surface inhomogeneously with some intermingled Wenzel and Cassie regions or (ii) the drop partially but homogeneously “wets” the roughened surface, where the top portion of the cavity is “filled” by liquid but the bottom remains dry. If there were surface impurities (such as dust particles), case i was observable under optical microscope; otherwise, neither case i nor ii could be unambiguously discerned by optical imaging. In keeping with the terminology of partial impalement, the *full impalement state* can be either a Wenzel or an impregnation state. Macroscopically, it suffices to note that any impalement of the roughness, partial or full, leads to a lower apparent contact angle and a dramatically larger contact angle hysteresis compared to the nonimpaled Cassie state.

It is important to note that, for one-tier roughnesses, the microtier surface was more susceptible to impalement than the nanotier surface, evident by the earlier transition from the

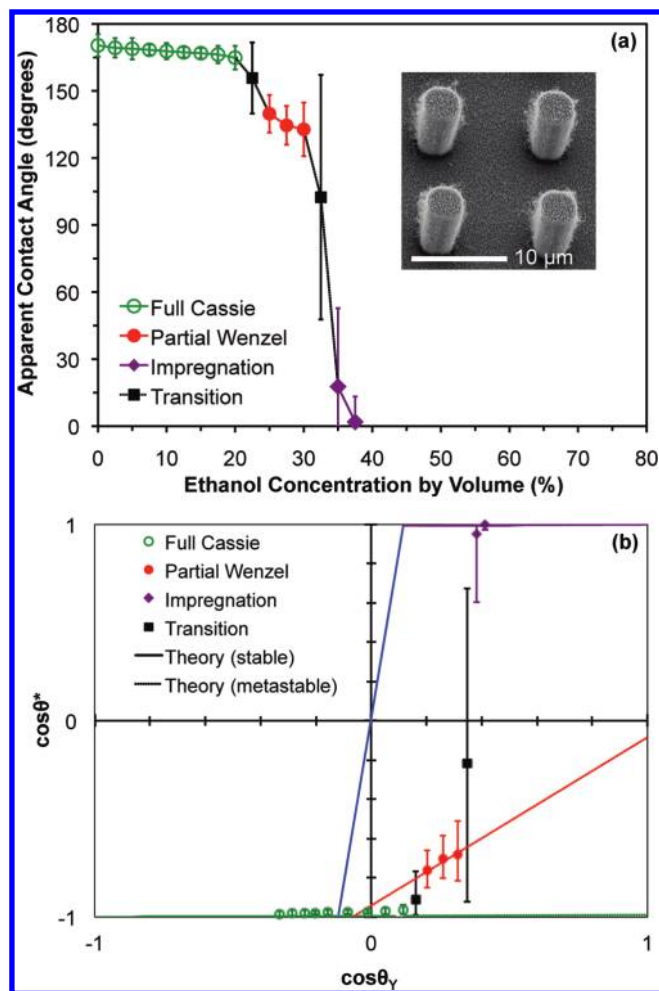


**Figure 5.** (a) Apparent contact angles of drops deposited on the two-tier surface, as a function of the ethanol concentration. Three different wetting states are evident from the sharp wetting transitions at  $22.5 \pm 2.5\%$  and  $32.5 \pm 2.5\%$  and are denoted as the full Cassie, partial Wenzel, and impregnation regimes. (b) The same data replotted on a cosine–cosine map. Theoretical lines of the wetting regimes eqs 4–7 are solid when energetically stable and are dotted when metastable.

Cassie state to the partial impalement state as the liquid wettability was increased. According to our model, the Cassie state was energetically stable on the nanotier surface while metastable on the microtier.

**3.2. Two-Tier Surface.** A variety of wetting states are possible on the two-tier surface, some illustrated in Figure 4. In this paper, the *partial Wenzel state* refers exclusively to a wetting state where one of the two tiers is fully wetted, while the other tier remains completely dry (i.e., one-tier Wenzel, one-tier Cassie). In the partial Wenzel regime, the wetting state was homogeneous within each tier, as sketched in Figure 4. In our terminology, the partial Wenzel state is a special subclass of the partial impalement state defined above.

On the two-tier surface, drops were again deposited with increasing ethanol concentration. Drops with ethanol concentrations up to 20% possessed apparent contact angles greater than  $160^\circ$  (Figure 5) and minimal contact angle hysteresis (Figure 6), indicating a *full Cassie state* atop both tiers of roughness. Importantly, drops in this regime experienced only a very weak decrease in apparent contact angle or increase in hysteresis as the ethanol

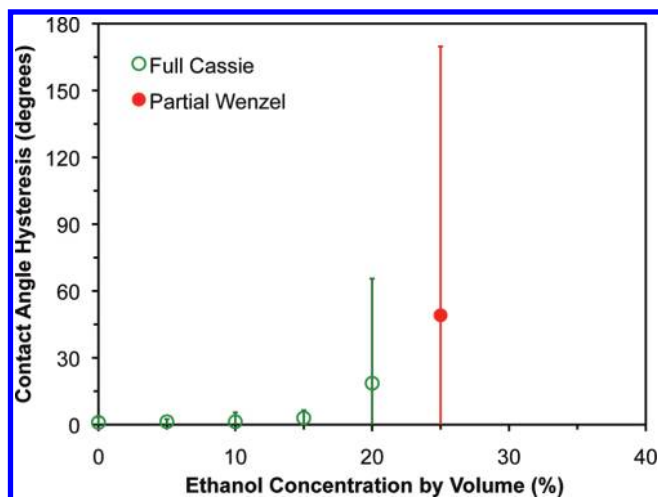


**Figure 6.** Contact angle hysteresis of the two-tier surface, as a function of the ethanol concentration. Drops in the full Cassie regime exhibit very small contact angle hysteresis, while the hysteresis in the partial Wenzel regime becomes too large to accurately measure.

concentration was increased, indicating no fundamental change in the full Cassie state of the drops. As the ethanol concentration increased beyond the full Cassie regime, the apparent contact angle sharply decreased at two distinct critical concentrations (Figure 5), each indicating a wetting transition.

At the first critical ethanol concentration of  $22.5 \pm 2.5\%$  (Figure 5), the apparent contact angle suddenly decreased despite the very slight change of 2.5% in ethanol concentration. Drops in the middle regime, ranging from 25% to 30% ethanol, exhibited lower contact angles of around  $140^\circ$  (Figure 5) and a dramatically larger contact angle hysteresis (Figure 6). While the large hysteresis and sudden change in contact angle indicated a wetting (impalement) transition, the apparent contact angle was still well above the Young's contact angle (which was already below  $90^\circ$ ), suggesting that some cavities were still dry underneath the drop. Therefore, drops in this middle regime seemed to be partially impaling the two-tier roughness. We shall show evidence below that this partial impalement state is in fact a partial Wenzel state.

After a second critical concentration of  $32.5 \pm 2.5\%$  (Figure 5), the apparent contact angle plummeted to hydrophilic values close to zero, indicating that the drops were now fully impaled. The visible liquid film surrounding the drop further suggested an impregnation state.

The two-stage wetting transition can be explained using the Wenzel and Cassie models, which are modified to account for the two-tier roughness.<sup>20</sup> For the two-tier chip used here, the side walls of the micropillars were approximately smooth with nearly no coating of the nanoscale roughness.<sup>22</sup> In this case, the apparent contact angle of drops in the full Cassie state can be estimated by modifying the Cassie equation

$$\cos \theta^* = \phi_m \phi_n (\cos \theta_Y + 1) - 1 \quad (4)$$

where  $\theta_Y$  is the Young's contact angle on a corresponding smooth surface and  $\phi_m$  and  $\phi_n$  represent the solid fractions of the microscale and nanoscale roughness, respectively.

Similarly, the apparent contact angle of partial Wenzel drops wetting only the microtier can be determined by modifying the

Wenzel equation

$$\cos \theta^* = (r_m + \phi_n - 1) \cos \theta_Y + \phi_n - 1 \quad (5)$$

where  $r_m$  represents the roughness of the microtier only. In the partial Wenzel relationship, the apparent contact angle ( $\cos \theta^*$ ) is a weighted average between the Young's contact angle ( $\cos \theta_Y$ ) and the contact angle between liquid and air ( $\cos 180^\circ$ ); the first weighing factor ( $r_m + \phi_n - 1$ ) accounts for the liquid–solid contact on the wetted micropillar sidewalls ( $r_m - 1$ ) and on top of the nanopillars ( $\phi_n$ ), while the second ( $1 - \phi_n$ ) accounts for the liquid–air contact. Note again that the sidewalls of the micropillars are not covered with nanopillars.

The full Wenzel state with both tiers wetted is given by

$$\cos \theta^* = (r_m + r_n - 1) \cos \theta_Y \quad (6)$$

where  $r_n$  represents the roughness of the nanotier only. The impregnation state has an impregnated liquid film surrounding the drop that fully impales both tiers, thus

$$\cos \theta^* = \phi_m \phi_n (\cos \theta_Y - 1) + 1 \quad (7)$$

In the impregnation equation, the surrounding film is assumed to have completely wetted both tiers of roughness.

As with the one-tier surfaces, Figure 5a was transformed into a cosine–cosine plot (Figure 5b). The full Cassie and partial Wenzel regimes extend far into the lower-right quadrant, which represents the metastable condition of a hydrophilic Young's contact angle leading to a hydrophobic apparent contact angle. The solid lines signify the stable theoretical values of the full Cassie, partial Wenzel, full Wenzel, and impregnation regimes respectively using eqs 4, 5, 6, and 7, while the dotted lines show the metastable theoretical values. The measured full Cassie state agrees with the theoretical stable and metastable full Cassie equation (eq 4). The measured partial Wenzel state agrees very well with the theoretical metastable state of the microtier-only impalement (eq 5). Finally, the fully impaled drops are well-modeled by the impregnation state (eq 7). Note that the second wetting transition occurs so quickly as to bypass the full Wenzel regime (Figure 5b).

The good agreement between the models and experiments suggests a two-stage wetting mechanism, which is consistent with the observation in section 3.1 that the microtier roughness is more susceptible to wetting than the nanotier. As further evidence, side-view optical imaging in Figure 7 also suggested that the microtier roughness was impaled at the first critical concentration, and the nanotier roughness was later invaded at the second wetting transition. Comparing a 20% full Cassie drop (Figure 7a) to a 25% partial Wenzel drop (Figure 7b), the bottom of the full Cassie drop was clearly resting atop the micropillars, while the partial Wenzel drop had penetrated the micropillars. Although the nanotier roughness was not optically resolvable, its impalement at 35% ethanol concentration could be deduced by comparing parts b and c of Figure 7: images of the microscale pillars were comparable, but the dramatic decrease in apparent contact angle in Figure 7c suggested that the nanopillars were additionally wetted. Unless there were surface impurities, inhomogeneous wetting with intermingled Wenzel and Cassie states was not observed on the visible micropillars. The sharpness of both wetting transitions suggests that first the microtier and then the nanotier were fully and uniformly impaled, with homogeneous wetting within each tier.

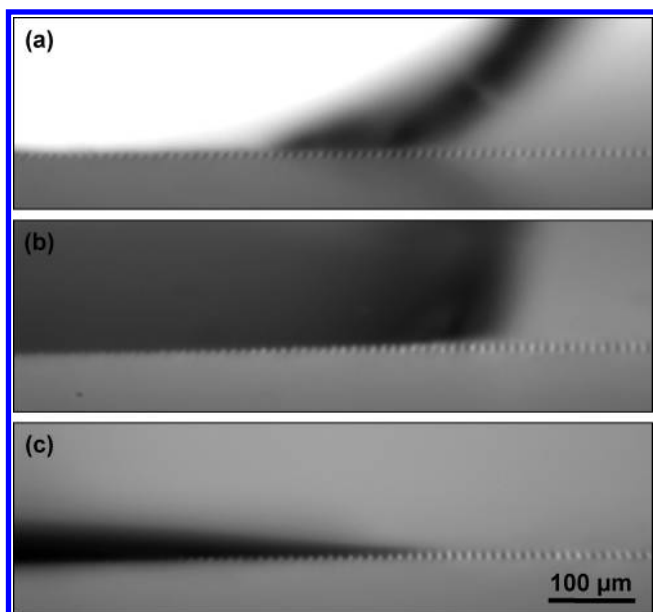


**Figure 7.** Side-view imaging of 2.5  $\mu\text{L}$  drops on the two-tier surface, where the center-to-center separation of the visible micropillars is 12  $\mu\text{m}$ : (a) 20% ethanol drop in the full Cassie state, visibly resting atop the micropillars; (b) 25% ethanol drop in the partial Wenzel state, wetting the microscale roughness; (c) 35% ethanol drop in the impregnation state, still wetting the microscale but additionally wetting the nanoscale, as inferred from the sudden decrease in the apparent contact angle. The same lighting and exposure time were used for all three images. The full Cassie image is significantly brighter because of the reflection at the air/water interface on top of the microscale cavities. Micropillars directly underneath the drops appear to be somewhat slanted due to the refraction of light through the drop.

The partial Wenzel drops reported here have large contact angle but high adhesion, a property combination also observed for water drops on rose petals.<sup>36,37</sup> The possibility of preferentially wetting one of the two tiers was recently reported,<sup>20,38</sup> but due to the randomness of the nanoscale roughness and the sparsity of data points, a distinct two-stage wetting transition was not demonstrated.

It should be noted that because the partial Wenzel, full Wenzel, and impregnation states all exhibit a pinned triple contact line (cf. Figure 6), more traditional wetting experiments such as measuring the contact diameter of an evaporating drop over time<sup>12,13</sup> can only convey the first wetting transition. Even when two-tier surfaces are employed, all that would be evident from the evaporation experiment is the wetting of the first tier of roughness when the contact line suddenly pins.<sup>21</sup> Once a drop is pinned, evaporation will decrease its contact angle to zero, regardless of any subsequent impalement into additional levels of roughness.

#### 4. DEWETTING TRANSITIONS

The wetting state on a hierarchical superhydrophobic surface has profound implications for the dewetting transition of (partially) impaled drops. For example, an impaled partial Wenzel drop on a lotus leaf can be transitioned to the full Cassie state through vibration-induced dewetting.<sup>29</sup> Here, the conditions for dewetting on the synthetic two-tier surface were studied with the corresponding one-tier surfaces used as control cases.

**4.1. One-Tier Surfaces.** For the microtier surface, a 1.5  $\mu\text{L}$  Cassie drop composed of 7.5% ethanol was easily removed from the surface upon vibration at 100 Hz and 0.12 mm peak-to-peak amplitude. In contrast, a 2  $\mu\text{L}$  partially impaled drop consisting of 12.5% ethanol could not be transitioned to the Cassie state, even at a much larger peak-to-peak amplitude of 0.66 mm, regardless of the duration of evaporation for the mixed drop to preferentially drive out ethanol prior to vibration.

Similar phenomena were observed for the nanotier surface; a 1.5  $\mu\text{L}$  ethanol drop composed of 12.5% ethanol was still in the Cassie state and could be immediately removed upon vibration at 100 Hz and 0.19 mm peak-to-peak amplitude. A 2  $\mu\text{L}$  partially impaled drop at 17.5% ethanol, however, was irreversibly impaled into the surface.

The superiority of the nanotier surface is evident from the dewetting experiments at 12.5% ethanol concentration: drops cannot be dewetted from the partial impalement state on the microtier surface but can be easily removed from the Cassie state on the nanotier surface.

**4.2. Two-Tier Surface.** For experiments presented in this section, an ethanol concentration was selected to first induce (partial or full) impalement of the two-tier substrate. A dewetting transition was then attempted after allowing the ethanol to preferentially evaporate from the drop (see section 2.3).

On the two-tier substrate, the wetting transition from the partial Wenzel to the full impalement state is well illustrated by the contrasting apparent contact angles at 27.5% and 32.5% (first frames of Figure 8a,b). It was previously determined that, for a 2.25  $\mu\text{L}$  drop with an initial ethanol concentration of 33% by volume, less than 10% of the drop would be ethanol after an evaporation time of 6 min.<sup>29</sup> The 27.5% drops used here were of identical volume, comparable apparent contact angle, and slightly lower ethanol concentration. Therefore, it can be assumed that the vast majority of the ethanol had evaporated after a wait time of 6 min, upon which mechanical vibration was applied. For the 32.5% drops, because of a dramatically different apparent contact angle, which affected the evaporation rate, a wide range of wait times from 4 to 10 min was attempted before vibration, with no appreciable change in results.

After evaporation, the impaled drop containing mainly water was then subjected to vertical mechanical vibration (Figure 8). Evident from the high-speed imaging, the partial Wenzel drop successfully dewetted to the full Cassie state (Figure 8a), while the full impalement drop remained stuck to the substrate at a considerably higher amplitude of vibration (Figure 8b). Figure 8a shows the dewetting of the partial Wenzel drop in approximately one period of oscillation, where the triple contact line completely receded from the rough surface, resulting in a permanent transition to the nonsticking Cassie state. The full impalement drop shown in Figure 8b could not be dewetted, even with an extremely high vibrational amplitude or with an air gun; both conditions would tear the top portion of the drop off, leaving the lower portion completely impaled in the surface.

The work required to dewet a partial Wenzel drop is given by the incremental work of adhesion.<sup>29</sup> The work of adhesion between the liquid and solid phase,  $w_{\text{SL}} = \gamma (1 + \cos \theta_{\text{Y}})$ , is the energy per unit area required to separate a flat liquid–solid interface into a double interface of liquid–vapor and solid–vapor. The incremental work of adhesion is motivated by the gradual receding of the contact line during the dewetting process, evident in Figure 8a. For partial Wenzel drops wetting the sides of the micropillars and resting atop the nanotubes, the

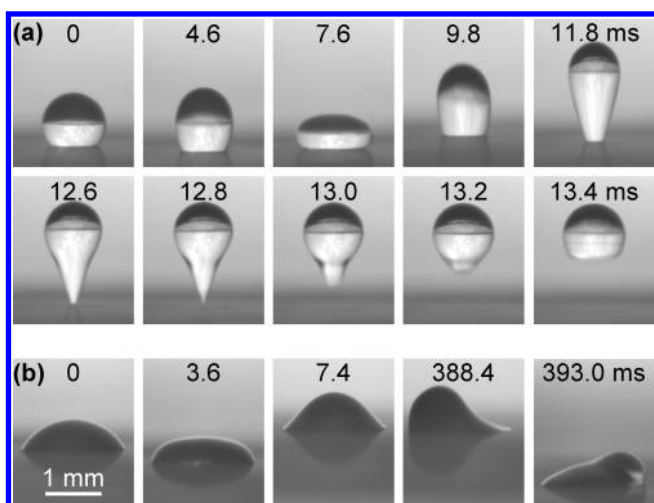


**Figure 8.** (a) Vibration-induced dewetting from the partial Wenzel to the full Cassie state on a two-tier surface. The drop was initially  $2.25 \mu\text{L}$  with 27.5% ethanol and was allowed to evaporate for 6 min until it was predominantly (>90%) water, rendering the Cassie state energetically stable. After evaporation, the remaining drop was vibrated at a frequency of 100 Hz and a peak-to-peak amplitude of 0.38 mm. (b) For a full Wenzel drop initially composed of 32.5% ethanol, no dewetting transition was observed at a much higher amplitude of 1.1 mm. The initiation of the vibration is time stamped zero. Available online as Videos S1 and S2 in the Supporting Information.

incremental work of adhesion for dewetting scales as

$$\Delta E_S \sim \gamma(r_m + \phi_n - 1)(1 + \cos \theta_Y)(2\pi a \Delta L_m) \quad (8)$$

where  $a$  is the contact radius of the drop with the substrate and  $\Delta L_m$  is the distance between two adjacent micropillars. Physically,  $\Delta E_S$  is the work of adhesion associated with the first step of dewetting, where the initial contact radius recedes by  $\Delta L_m$ , the intermicropillar separation which stipulates the minimum shrinkage of the contact radius. Note that the same geometrical factor  $(r_m + \phi_n - 1)$  accounting for the liquid–solid contact appears in both the wetting eq 5 and dewetting eq 8.

The kinetic energy imparted to the drop by the speaker is maximized at resonance. The imparted energy scales as

$$E_K \sim \frac{1}{2} \rho V (2\pi f A)^2 \quad (9)$$

where  $\rho$  and  $V$  are the density and volume of the drop, and  $f$  and  $2A$  are the frequency and peak-to-peak amplitude of vibration. When the full Cassie state is the energetically favorable configuration and sufficient energy is supplied to overcome the incremental work of adhesion,

$$E_K \gtrsim \Delta E_S \quad (10)$$

the contact line of the partial Wenzel drop will continuously shrink, eventually leading to a transition to the full Cassie state. Taking Figure 8a, for example, the imparted energy ( $E_K = 5.7 \text{ nJ}$ ) is sufficient to overcome the incremental work of adhesion ( $\Delta E_S = 1.6 \text{ nJ}$ ) to complete the dewetting transition. A more rigorous test of this scaling argument (eq 10) can be found in ref 29 for the threshold conditions to dewet lotus leaves.

Since the ethanol concentration of the drops in Figure 8a,b was different by only 5%, the drastic difference in dewetting behavior should be attributed to the contrast between the partial Wenzel

and full impalement states (Figure 7b,c). Partial Wenzel drops wetting only the micropillars could be dewetted to the full Cassie state, while full impalement drops wetting both tiers were irreversibly wetted. This finding is along the same line as a previous study of drops impacting a hierarchical surface, in which the incoming drops successfully rebound when only the microscale is wetted during collision, but not when the nanoscale is additionally wetted at higher impact speeds.<sup>39</sup> Another study of electrowetting on hierarchical surfaces reports that the electrically induced wetting is only reversible when the apparent contact angle is kept above  $140^\circ$  or so,<sup>40</sup> which agrees well with the contact angle of the partial Wenzel drops reported here.

## 5. DISCUSSION

It remains a challenge to unambiguously image and probe the wetting state within microscale and nanoscale cavities. Synthesizing the experimental evidence presented above, we provide further discussions on our interpretations of the wetting states and their relation to dewetting.

**5.1. Inference of the Partial Wenzel State.** From experimental observations, three regimes can be distinguished: (i) full Cassie state, with a close to  $180^\circ$  apparent contact angle and a nearly zero hysteresis; (ii) partial impalement state, with a dramatic increase in contact angle hysteresis (Figure 6); and (iii) full impalement state, with a close to  $0^\circ$  apparent contact angle (Figure 7c). The full impalement regime can be further divided into the full Wenzel and impregnation states, the latter being signified by an impregnated liquid film that is usually visible. The partial impalement state encompasses many possible wetting configurations (some discussed in section 3.1), but the details can only be inferred from experimental measurements.

The inference of the partial Wenzel (i.e., microtier Wenzel, nanotier Cassie) state is pivotal to interpreting both wetting and dewetting experiments on the two-tier surface. The partial Wenzel state is supported by the two distinct and sharp transitions in the apparent contact angle (Figure 5a). The first transition is further attributed to microtier wetting, because side-view imaging indicated homogeneous impalement of the microtier at the first critical ethanol concentration (Figure 7). This attribution is consistent with the fact that the microtier-only surface (Figure 2) was more susceptible to wetting compared to its nanotier counterpart (Figure 3). In addition, the partial Wenzel model (eq 5) quantitatively predicts the apparent contact angle measured in this intermediate regime (Figure 5b).

The two-stage wetting model is corroborated by the possibility to dewet the two-tier surface in the partial Wenzel state by vibration (Figure 8) and is also quantitatively supported by the incremental work of adhesion model (eqs 8–10) predicting the threshold dewetting conditions (see also ref 29). Note that the partial Wenzel state is a special subset of the much broader partial impalement state. The former is signified by the ability to dewet to the full Cassie state by vibration.

**5.2. Conditions for Vibration-Induced Dewetting.** The partial impalement and full impalement states are irreversible for one-tier surfaces, at least as far as vibration-induced dewetting is concerned. In contrast, the partial Wenzel state on the two-tier surface can be dewetted to the full Cassie state. The difference in the dewetting capability cannot be explained by energetic considerations alone, including surface energy minimization (solid lines in Figures 2b, 3b, and 5b) and the incremental work of adhesion model (eqs 8–10). Otherwise, the nanotier-only

surface (on which Cassie state is favorable for pure water) could be dewetted with even lower external energy supply, as the internanopillar separation is much lower than the corresponding micropillar separation ( $\Delta L_m$ ). In addition, the energetic argument could not explain the experimental fact that fully impaled drops cannot be dewetted from the two-tier surface.

In the partial Wenzel state, we believe that the microtier is impaled but the nanotier remains intact in the Cassie state. We speculate that the *intact* nanotier cavities serve as “nuclei” for the dewetting process, perhaps by coupling external energy in through the oscillation of the air/liquid interface.

## 6. CONCLUSION

In conclusion, two distinct wetting transitions are observed on a superhydrophobic surface with hierarchical two-tier roughness. For aqueous drops with increasing wettability (by increasing the ethanol concentration), the first transition from the full Cassie to partial Wenzel state occurs when the microtier roughness is wetted, and the second transition from the partial Wenzel to the full impalement state occurs when the nanotier is additionally wetted. The partial Wenzel state can be reverted to the full Cassie state by vibration-induced dewetting (after ethanol has preferentially evaporated), but the full impalement state is irreversible.

Compared to the one-tier surfaces, the two-tier one is superior in resisting wetting and facilitating dewetting. The critical ethanol concentration for liquid impalement was much larger on the two-tier roughness. After (partial) impalement, the vibration-induced dewetting was only possible on the two-tier surface. The superiority is ultimately related to the mechanism of the two-tier design, which remains an open question to date. By experimentally identifying that microscale and nanoscale roughnesses are not necessarily wetted at the same time, our work will hopefully contribute to the mechanistic understanding of wetting on hierarchical roughnesses.

## ■ ASSOCIATED CONTENT

**S** **Supporting Information.** Videos S1 and S2 correspond to the external vibration of a partial Wenzel drop (Figure 8a) and a full impalement drop on the two-tier surface (Figure 8b), respectively. This material is available free of charge via the Internet at <http://pubs.acs.org>.

## ■ AUTHOR INFORMATION

### Corresponding Author

\*E-mail: [chuanhua.chen@duke.edu](mailto:chuanhua.chen@duke.edu).

## ■ ACKNOWLEDGMENT

This work was funded in part by a Young Faculty Award from the Defense Advanced Research Projects Agency (Grant No. N66001-10-1-4048), a Ralph E. Powe Junior Faculty Enhancement Award from Oak Ridge Associated Universities, and an award from the North Carolina Space Grant New Investigators Program. C.H.B. was supported by the Pratt Fellows Program at Duke University. C.R.P. was supported by the National Science Foundation (Grant No. 0754963) as part of the Research Experiences for Undergraduates Program of Duke's Pratt School of Engineering. The authors thank M. Absher for administrating both fellowships and Y. Zhao for helpful discussions.

## ■ REFERENCES

- (1) Neinhuis, C.; Barthlott, W. *Ann. Bot.* **1997**, *79*, 667–677.
- (2) Gao, X.; Jiang, L. *Nature* **2004**, *432*, 36.
- (3) Quere, D. *Rep. Prog. Phys.* **2005**, *68*, 2495–2532.
- (4) Cassie, A. B. D.; Baxter, S. *Trans. Faraday Soc.* **1944**, *40*, 546–551.
- (5) Wenzel, R. N. *Ind. Eng. Chem.* **1936**, *28*, 988–994.
- (6) Bico, J.; Marzolin, C.; Quere, D. *Europhys. Lett.* **1999**, *47*, 220–226.
- (7) Oner, D.; McCarthy, T. J. *Langmuir* **2000**, *16*, 7777–7782.
- (8) Feng, L.; Li, S.; Li, H.; Zhai, J.; Song, Y.; Jiang, L.; Zhu, D. *Angew. Chem., Int. Ed.* **2002**, *41*, 1221–1223.
- (9) Lau, K. K. S.; Bico, J.; Teo, K. B. K.; Chhowalla, M.; Amaratunga, G. A. J.; Milne, W. I.; McKinley, G. H.; Gleason, K. K. *Nano Lett.* **2003**, *3*, 1701–1705.
- (10) Liu, K.; Yao, X.; Jiang, L. *Chem. Soc. Rev.* **2010**, *39*, 3240–3255.
- (11) Lafuma, A.; Quere, D. *Nat. Mater.* **2003**, *2*, 457–460.
- (12) McHale, G.; Aqil, S.; Shirtcliffe, N. J.; Newton, M. I.; Erbil, H. Y. *Langmuir* **2005**, *21*, 11053–11060.
- (13) Reyssat, M.; Yeomans, J. M.; Quere, D. *Europhys. Lett.* **2008**, *81*, 26006.
- (14) Reyssat, M.; Pepin, A.; Marty, F.; Chen, Y.; Quere, D. *Europhys. Lett.* **2006**, *74*, 306–312.
- (15) Bormashenko, E.; Pogreb, R.; Whyman, G.; Erlich, M. *Langmuir* **2007**, *23*, 12217–12221.
- (16) Narhe, R. D.; Beysens, D. A. *Phys. Rev. Lett.* **2004**, *93*, 076103.
- (17) Wier, K. A.; McCarthy, T. J. *Langmuir* **2006**, *22*, 2433–2436.
- (18) Dorrer, C.; Ruhe, J. *Langmuir* **2007**, *23*, 3820–3824.
- (19) Koch, K.; Bhushan, B.; Jung, Y. C.; Barthlott, W. *Soft Matter* **2009**, *5*, 1386–1393.
- (20) Cha, T. G.; Yi, J. W.; Moon, M. W.; Lee, K. R.; Kim, H. Y. *Langmuir* **2010**, *26*, 8319–8326.
- (21) Chen, C. H.; Cai, Q.; Chen, C. L. *ASME International Conference on Micro/Nano Heat Transfer*; Tainan, Taiwan, 2008; #52355.
- (22) Chen, C. H.; Cai, Q.; Tsai, C.; Chen, C. L.; Xiong, G.; Yu, Y.; Ren, Z. *Appl. Phys. Lett.* **2007**, *90*, 173108.
- (23) Herminghaus, S. *Europhys. Lett.* **2000**, *52*, 165–170.
- (24) Patankar, N. A. *Langmuir* **2004**, *20*, 8209–8213.
- (25) Nosonovsky, M. *Langmuir* **2007**, *23*, 3157–3161.
- (26) Su, Y.; Ji, B.; Zhang, K.; Gao, H.; Huang, Y.; Hwang, K. *Langmuir* **2010**, *26*, 4984–4989.
- (27) Quere, D. *Annu. Rev. Mater. Res.* **2008**, *38*, 71–99.
- (28) Cheng, Y. T.; Rodak, D. E. *Appl. Phys. Lett.* **2005**, *86*, 144101.
- (29) Boreyko, J. B.; Chen, C. H. *Phys. Rev. Lett.* **2009**, *103*, 174502.
- (30) Boreyko, J. B.; Chen, C. H. *Phys. Rev. Lett.* **2009**, *103*, 184501.
- (31) Boreyko, J. B.; Chen, C. H. *Phys. Fluids* **2010**, *22*, 091110.
- (32) Vazquez, G.; Alvarez, E.; Navaza, J. M. *J. Chem. Eng. Data* **1995**, *40*, 611–614.
- (33) Noblin, X.; Buguin, A.; Brochard-Wyart, F. *Eur. Phys. J. E* **2004**, *14*, 395–404.
- (34) Frohn, A.; Roth, N. *Dynamics of Droplets*; Springer: New York, 2000.
- (35) Bico, J.; Tordeux, C.; Quere, D. *Europhys. Lett.* **2001**, *55*, 214–220.
- (36) Feng, L.; Zhang, Y.; Xi, J.; Zhu, Y.; Wang, N.; Xia, F.; Jiang, L. *Langmuir* **2008**, *24*, 4114–4119.
- (37) Bhushan, B.; Her, E. K. *Langmuir* **2010**, *26*, 8207–8217.
- (38) Wu, A. H. F.; Cho, K. L.; Liaw, I. I.; Moran, G.; Kirby, N.; Lamb, R. N. *Faraday Discuss.* **2010**, *146*, 223–232.
- (39) Chen, M. H.; Hsu, T. H.; Chuang, Y. J.; Tseng, F. G. *Appl. Phys. Lett.* **2009**, *95*, 023702.
- (40) Lapiere, F.; Brunet, P.; Coffinier, Y.; Thomy, V.; Blossey, R.; Boukherroub, R. *Faraday Discuss.* **2010**, *146*, 125–139.